Polymer-protected gold nanoparticles for photothermal treatment of Ehrlich Adenocarcinoma: in vitro and in vivo studies

Polymer-protected gold nanoparticles for photothermal treatment of Ehrlich adenocarcinoma: *In vitro* and *in vivo* studies

Gulnur S. Tatykhanova[1,3], Rysgul N. Tuleyeva[1,2], Zhanara A. Nurakhmetova[1], Nargiz N. Gizatullina[1], Vladimir K. Krasnoshtanov[4], Daulet B. Kaldybekov[1,2,6] , Vladimir O. Aseyev[5], Vitaliy V. Khutoryanskiy[6], Sarkyt E. Kudaibergenov[1*]*

G.S. Tatykhanova, R.N. Tuleyeva, Zh.A. Nurakhmetova, N.N. Gizatullina, S.E. Kudaibergenov

[1] Institute of Polymer Materials and Technology, 050019 Almaty, Kazakhstan, E-mail: skudai@mail.ru

R.N. Tuleyeva, D.B. Kaldybekov

[2] Department of Chemistry and Chemical Technology, Al-Farabi Kazakh National University, 050040 Almaty, Kazakhstan

G.S. Tatykhanova

[3] Satbayev University, 050013 Almaty, Kazakhstan, E-mail: gulnur-ts81@yandex.kz

V.K. Krasnoshtanov

[4] Kazakh Research Institute of Oncology and Radiology, 050022 Almaty, Kazakhstan

V.O. Aseyev

[5] Department of Chemistry, University of Helsinki, 00014 Helsinki, Finland

V.V. Khutoryanskiy

[6] Reading School of Pharmacy, University of Reading, Whiteknights, RG6 6DX Reading, United Kingdom

Keywords: gold nanoparticles, gold nanospheres, gold nanorods, surface plasmon resonance (SPR), photothermal therapy (PTT), Ehrlich cancer cells.

Abstract

Photothermal therapy (PTT) has been recognized as an effective tool for the treatment of cancer and it has attracted considerable attention of scientists. In this work, gold nanospheres (AuNSs) and gold nanorods (AuNRs) stabilized using poly(*N*-vinylpyrrolidone) (PVP), pristine gellan gum (PGG), and poly(2-ethyl-2-oxazoline)-grafted gellan gum (GG-*g*-PEtOx) were synthesized and evaluated as PTT agents in Ehrlich cancer cells. The physicochemical

characteristics of these AuNSs and AuNRs, including their surface plasmon resonance absorption spectra, size, zeta potential, and aspect ratio have been studied using UV/Vis-spectroscopy, dynamic light scattering, zeta potential, transmission electron microscopy, and optical microscopy techniques. The polymer-protected AuNSs exhibited light-to-heat conversion, raising the temperature from 37 to 43 °C when irradiated using a visible light source. In the case of AuNSs, considerable damage to Ehrlich cancer cells was observed following irradiation and 40 days of examination. However, with regards to AuNSs, the damage to Ehrlich cancer cells was slightly lower than observed in AuNRs. *In vivo* experiments demonstrated that laser irradiation of tumors in mice after injecting AuNSs led to a statistically significant decrease in tumor size as compared to those not irradiated and the control samples.

1. Introduction

Cancer is a multifaceted disease characterized by uncontrolled growth and spread of abnormal cells in the body and is one of the leading causes of human morbidity and mortality worldwide.[1–4] Unfortunately, due to the heterogeneous nature of cancer, which poses a significant public health challenge, there are currently no fully inclusive approaches to effectively treat this condition.[5] The primary modalities currently employed for cancer treatment include chemotherapy, radiation therapy, immunotherapy, and surgery. These methods have become widely used in clinical practice for decades. However, cancer patients undergoing these therapies often experience significant adverse effects.[6] For this reason, the majority of studies in cancer therapy are focused on the development of alternative therapies that can complement or even substitute the existing therapies. The goal is to improve their efficacy and minimize any potential side effects they may have on patients. These methods ideally should selectively eliminate cancerous cells only, without damaging healthy cells.[7,8] Among the advanced phototherapy methods for treating cancer, photothermal therapy (PTT) offers a great advantage due to its non-invasive nature and selective therapeutic potential for different cancers. PTT has several advantages including the ability to externally irradiate tumors, which means the therapy can be applied from outside the body. PTT is also associated with limited complications, meaning it has a lower risk of side effects compared to other cancer therapies. Additionally, PTT offers enhanced selectivity, meaning it can specifically target cancer cells while minimizing the damage to normal cells. Another benefit of PTT is a relatively quick patient recovery, implying that they may experience a faster recuperation period after undergoing PTT. In phototherapy, certain wavelengths of light within the visible and near-infrared resonance (NIR) bands are utilized to heat photothermal agents such as nanoparticles.

This leads to a localized increase in the temperature of specific tissues resulting in the elimination of malignant cells in those tissues. The higher sensitivity of cancer cells to temperature elevation results in their increased susceptibility to the effects of heat compared to normal cells. Moreover, an exposure to an external laser with adjustable dosing facilitates the selective eradication of various types of cancer cells while minimizing the damage to the surrounding healthy tissues.[9–14]

Gold nanoparticles (AuNPs) are considered to be the foremost photothermal agents used in PTT treatment. These nanoparticles have an important attribute such as a high light-to-heat conversion efficiency, which makes them particularly effective in converting light energy into heat. In PTT, visible and NIR laser lights are employed to activate and stimulate AuNPs, which cause the nanoparticles to resonate and generate heat, thus enabling localized heating of the targeted tumor tissues. The application of AuNPs as photothermal agents provides enhanced therapeutic outcomes due to the possibility of their direct injection into the tumor, while minimizing non-specific distribution in the body. Furthermore, these nanoparticles can be safely eliminated from the body after completing the therapy.[15–17]

AuNPs exhibit distinctive physicochemical properties such as a possibility for localized surface plasmon resonance (LSPR). The LSPR phenomenon facilitates interactions between incident light and the electrons in the conduction band on the surface of AuNPs.[18–20] The optical properties of AuNPs are dependent on their dimensions. The LSPR properties can be altered by modifying the shape and size of AuNPs. This enables the use of different wavelengths of light, including those in the NIR and visible spectra for achieving localized heating effects.[21–24] Therefore, the ability to tune the LSPR properties of AuNPs through size and shape manipulation offers flexibility in designing AuNPs for specific applications that require interaction with different wavelengths of light. Visible light has limited penetration ability into biological tissues compared to NIR light. This property makes visible light more suitable for certain medical procedures that require higher precision.[25–28]

Small spherical gold nanoparticles are easy to produce.[12] They are less toxic than particles of large size and show improved photoconversion capability that may profit from the irradiation with the visible light using standard surgical green lasers. In particular, the efficiency of light-to-heat conversion (photoconversion at 530 nm) of 14 nm AuNSs irradiated in the visible region and its application to selectively obliterate cancer cells using breast cancer as model was shown. Thus, the AuNSs with diameters ranging from 10 to 30 nm were considered non-toxic due to such properties, as stability, cellular uptake efficiency, and favourable clearance mechanism. They were recognized as ideal photothermal agents for biomedical

applications [29,30] and demonstrated a characteristic LSPR band around 520 nm, *i.e*. in the visible region of the spectrum, with an efficient light-to-heat conversion.[31,32] As such, AuNSs as photothermal agents, are an efficient way to induce precise heating leading to less damage to surrounding tissues, while destroying malignant, which are thermosensitive cells [33,34].

Many synthetic and natural polymers can function as both reducing and capping agents to form AuNPs.[35,36] According to literature, the efficacy of PTT with regards to the antitumor activity of AuNSs and AuNRs, among other noble and transition metal nanoparticles stabilized with natural and/or synthetic polymers, has been studied with respect to melanoma,[37] 4T1 and HeLa cells,[38] 4T1 murine breast tumor cells,[39] U87 MG human glioblastoma cell,[40] and transplanted liver tumor.[41]

In the present work, AuNSs and AuNRs stabilized using poly(*N*-vinylpyrrolidone) (PVP), pristine gellan gum (PGG), and poly(2-ethyl-2-oxazoline)-grafted gellan gum (GG-*g*-PEtOx) were prepared and characterized for their size and morphology using dynamic light scattering (DLS) and transmission electron microscopy (TEM). Coating and stabilization of AuNPs and AuNRs by biocompatible, non-toxic, and biodegradable polymers, such as poly(N-vinylpyrrolidone) and gellan, allows to preserve the colloidal gold nanoparticles in aqueous solution for an extended period and to prepare effective photothermal agent for the treatment of cancer cells.[42–50] Polymer-protected gold nanoparticles were produced through one-pot and growth seeding methods in aqueous solutions. These particles were observed to exhibit temperature-dependent changes and high stability over a period of 36 days, thus making them suitable for application in photothermal therapy. The protocols have been developed herein for the evaluation of the photothermal conversion ability of AuNSs and AuNRs when irradiated using visible and NIR laser light sources. The potential use of AuNSs and AuNRs in PTT treatment was tested both *in vitro* and *in vivo* against Ehrlich cancer cells. Ehrlich ascites carcinoma is a well-established murine model used for studying breast cancer. [51,52] It represents hyperdiploid and an undifferentiated carcinoma with 100% malignancy, short life span, high transplantable capability, and rapid proliferation. From 2010 until now, publications that mention Ehrlich tumors increases. This is due to the systematic alterations induced by the tumors, the sensitivity of the tumor cells to chemotherapies and the antitumor potential of synthetic and natural products.

It is known[53] that malignant cells require large amounts of monosaccharide uptake in order to sustain their accelerated growth and division in comparison to that of healthy cells. We hypothesize that gellan gum composed of tetrasaccharide repeating units (1,3-β-D-glucose, 1,4-β-D-glucuronic acid, 1,4-β-D-glucose, and 1,4-α-L-rhamnose) may function as a “food” for

cancer cells to support their accelerated growth. It is supposed that the cancer cells, feeding on tetrasaccharides, consume them and thereby "bare" gold nanoparticles that have been stabilized by the polysaccharide – gellan. Gold nanoparticles lacking a protective shell consisting of gellan will be forced to adsorb on cancer cells in order to minimize the free energy of the nanoparticles. Irradiation of these gold nanoparticles, attached to the cancerous cells, with appropriate laser light can induce local heating due to the localized surface plasmon resonance (LSPR) and hyperthermia causing apoptosis of the cancer cells. In addition, gellan gum grafted with poly(2-ethyl-2-oxazoline) (GG-*g*-PEtOx) could act as a bioadhesive polymer[54] and enhance its mucus-penetrating properties.[55] Therefore, coating or conjugating gold particles with these polymers could facilitate the adhesion of gold nanoparticles to the mucosal surface of tumors or their penetration into tumors. This process may prolong the efficacy of photothermal therapy (PTT) by ensuring better localization of gold nanoparticles within the tumor tissue.

2. Experimental Part

2.1. Materials

A standard aqueous solution of tetrachloroauric acid ($HAuCl_4$) with a concentration of 100 mg/mL, cetyltrimethylammonium bromide (CTAB, 99%), sodium borohydride ($NaBH_4$, 98.5%), ascorbic acid, poly(N-vinylpyrrolidone) (PVP) with Mn = 10 and 40 kDa, and Hanks' balanced salt solution (HBSS buffer) were purchased from Sigma-Aldrich (Germany). Gellan gum with Mw 500 kDa was purchased from Zhejiang DSM Zhongken Biotechnology Co., Ltd. (China). Poly(2-ethyl-2-oxazoline)-grafted gellan gum (GG-*g*-PEtOx) was kindly provided by the authors.[56] Depending on the grafting density, the GG-*g*-PEtOx samples are abbreviated as G2, G3, and G12. Grafting density is given as the number of repeating units, where each gellan gum consists of four sugar units, per one PEtOx grafted chain. Thus, on average, every 12th repeating unit (equivalent to 12×4 sugar units) in G12 copolymer contains one PEtOx grafted chain. Potassium hydroxide, silver nitrate, and all other chemicals were of analytical grade and used as received.

2.2. Methods

2.2.1. Synthesis of AuNSs and AuNRs

Spherical AuNPs (or AuNSs) stabilized by PVP, PGG, and GG-g-PEtOx were prepared using a "one-pot" synthetic method as described previously.[57] Briefly, a mixture consisting of polymer solutions with different concentrations (either 4% PVPs; 0.5% PGG; or 2% of each G12, G3, G2), 5 mL of $HAuCl_4$ (100 mg/mL) and 4 mL of 0.5 M KOH was combined, agitated,

and heated up to 100 °C for 3–5 min in an Anton Paar Monowave 50 microwave reactor (Graz, Austria) equipped with a temperature and time controller. Consequently, tinted solutions, varying in color from yellow to dark red or purple, were produced due to the formation of AuNSs. The initial solution with pH 12 decreased down to pH 8 following the dialysis (cellulose membrane with molecular weight cut-off 12-14 kDa) against deionized water.

In order to prepare AuNRs, the seed-mediated growth technique was employed.[57] Initially, a solution comprising 5 mL of 0.2 M cetyltrimethylammonium bromide (CTAB) was combined with 5 mL of 0.5 mM $HAuCl_4$ and stirred. Subsequently, 0.6 mL of cold 0.01 M $NaBH_4$ was introduced, resulting in the formation of a brownish-yellow solution containing AuNSs. Concurrently, a mixture composed of CTAB (0.2 M; 30 mL), $AgNO_3$ (4 mM; 1.5 mL), and $HAuCl_4$ (1 mM; 30 mL) was gently mixed, and 78.8 M (0.42 mL) ascorbic acid was added. Ascorbic acid was acting as a mild reducing agent, causing the color of the growth solution to change from dark yellow to colorless. Finally, the first seed solution (72 µL) was added to the second growth solution, and the mixture was allowed to incubate at 30 °C overnight. Consequently, a crimson solution containing AuNRs was generated. To eliminate by-products and CTAB from the AuNRs, the solution underwent centrifugation at 10650 rpm for 30 min using an Eppendorf 5810R centrifuge (Tuttlingen, Germany). The resulting precipitate was re-dispersed by adding 3 mL of deionized water and centrifuged again at 10650 rpm for 15 min. After undergoing washing procedure thrice, the AuNRs were re-dispersed and stabilized in 5 mL of designated polymer solutions and then dialyzed using a cellulose membrane (molecular weight cut-off 12-14 kDa) against deionized water.

2.2.2. Characterization

Absorption spectra of AuNSs and AuNRs were recorded using a Specord 210 plus BU UV/Vis-spectrophotometer (Jena, Germany). The mean hydrodynamic size of gold nanoparticles in solution, their polydispersity index (PDI) and zeta potential values were determined using dynamic light scattering (DLS) and electrophoretic measurements with a Malvern Zetasizer Nano ZS90 (Malvern Instruments, UK) at 25 °C. Gold nanoparticles were imaged using a JEOL JEM-1400Plus (JOEL Ltd., Japan) transmission electron microscope (TEM) operated at an acceleration voltage of 120 kV. TEM grids were prepared by placing 10 µL of the diluted sample solutions on a carbon-coated copper grid and evaporating the solution at room temperature completely. The concentrations of AuNSs and AuNRs solutions stabilized with the polymers were quantified using an Agilent 7500 ICP-MS inductively coupled plasma mass spectrometer (Agilent Technologies, USA).

2.2.3. Study of ex vivo photothermal effect of AuNSs induced by visible light irradiation

The porcine stomach tissue was used as a model of skin to study *ex vivo* photothermal effect of AuNSs when exposed to irradiation. Porcine stomach tissues were received from Altyn-Orda Abattoirs (Almaty, Kazakhstan) immediately after animal slaughter, carefully packed, transported to the laboratory in cold plastic containers, and used within 24 h of retrieval. Tissue samples (cut into ≈ 3 × 3 cm) were placed in Petri dishes, and with the help of a marker pen, an area to be exposed to irradiation was highlighted. Using a sterile syringe, 0.5 mL of polymer-coated AuNSs dispersion was injected interstitially in the porcine stomach tissue. The concentration of AuNSs in the colloidal solution was determined to be ~45 μg/mL. Irradiation of AuNSs was carried out using a physiotherapeutic Lasmik® laser apparatus (Lazmik Ltd., Russia) (Figure S1A). Matrix LED heads operated at 530 and 780 nm wavelengths were used. Experiments with irradiation were performed within an incubator at 37 °C with a relative humidity of 80% (Figure S1B). The temperature was measured every 5 min using a VT04 visual infrared thermometer (Fluke VT02 Visual IR Thermometer, Everett, WA, USA). The irradiation was carried out for 60 min. All experiments were performed in triplicate and the mean ± standard deviation (SD) values were calculated.

2.2.4. Irradiation of Ehrlich cancer cells

Ehrlich cells were received from the cell culture collection of the Kazakh Research Institute of Oncology and Radiology (Almaty, Kazakhstan). The ascites form of a transplanted Ehrlich tumor strain was used to study the photothermal effect of AuNPs on cancer cells. The tumor cells were transplanted intraperitoneally into CD-1 mice. The material was extracted on the 10th day after transplantation. The concentration of cells was determined to be 100 million/mL. In this experiment, a suspension of biomaterial was prepared from 1 mL suspension of Ehrlich tumor cells and 9 mL of HBSS buffer solution (Hanks culture medium). Next, 1 mL of the suspension was aspirated and then mixed with 1 mL of either AuNPs (~45 μg/mL) or AuNRs (~179 μg/mL) solutions. The resulting mixture was subsequently irradiated for 60 min using matrix LED heads operated at λ = 530 and 780 nm. The cover glass was placed on the grid of a Goryaev chamber. Then, 5-10 μL of cell suspension was transferred to the edge of the cover glass in the chamber. Afterwards, microphotographs of the cells were taken at 40× magnification using a Nikon Eclipse LV150N microscope (Tokyo, Japan), equipped with a Motic digital camera, and the cells were counted in Goryaev chamber manually before and after irradiation. The average number of cells in one square of grids and in one mL of suspension was calculated, considering the area of the square. The cells were maintained in an incubator at

37 °C and in the dark throughout the experimental period. In order to evaluate the long-term photothermal effect of polymer-coated AuNSs on Ehrlich cancer cells, the cells death was observed over a 40-days period. All measurements were conducted in triplicate and the mean ± standard error of the mean (SEM, n = 10) values were calculated and then evaluated statistically.

2.2.5. Study of in vivo photothermal effect of AuNSs induced by visible light irradiation

All animal experiments were conducted in compliance with the protocol approved by the local ethical committee (LEC) at the Kazakh Research Institute of Oncology and Radiology (Protocol No.5-2021, December 10, 2021).

For the *in vivo* experiments, 18 CD-1 male mice of 23–25 g weight and 60 days of age were selected. Tumor cell transplantation into the animals was accomplished through subcutaneous injection of 5×10^6 tumor cells. The experiments commenced 10 days later when the tumors reached a size of about 4-5 mm in diameter. However, throughout the experiment, some mice developed purulence and so the other 3 mice were excluded from the experiment due to this condition. The mice were divided into 3 groups: Group 1 consisted of 5 control animals, with no AuNSs solution injected and no exposure to irradiation; Group 2 included 5 animals with AuNSs solution injected, but no irradiation treatment; and Group 3 involved 5 animals with AuNSs solution injected and with irradiation treatment.

Prior to commencing each experiment, hair from the surface of the skin covering the tumor was removed, then intratumoral injection of 50 μL of AuNSs-PVP (40 kDa) was administered. The concentration of AuNSs in the suspension was ~45 μg/mL. After 25 min, the tumor node was subjected to a daily laser exposure for 30 min over a period of 7 days. Taking into account 10 days of inoculation and 7 days of laser exposure the total experimental time duration was 17 days. According to the protocols reported in,[58] the experiment associated with an increase in the tumor weight was conducted for 20 days until the animals were sacrificed. A Polyaron LG-75 helium-neon laser at a wavelength of 633 nm and emissive power of 25 mW (Kyiv, Ukraine) was used in the experiments. Throughout the experiment, the tumor size was measured daily using a caliper. Following the internationally recognized guidelines established by the Council for International Organizations of Medical Sciences (CIOMS) for biomedical research involving animals, the mice were euthanized prior to surgical removal of tumor tissues. The tumors were extracted from the peritoneum by dissection with a subsequent weighing on the ninth day.

2.2.6. Statistical analysis

The data were presented as mean values ± SDs and/or SEMs and assessed for significance using a one-way and two-way analysis of variance (ANOVA) followed by Bonferroni post hoc test, where $p < 0.05$ was considered as the statistical significance difference (GraphPad Prism software, version 7.0; San Diego, CA, USA).

3. Results and Discussion

3.1. Physicochemical characterization of nanoparticles

Poly(N-vinylpyrrolidone) (PVP) with Mn 10 and 40 kDa, pristine gellan gum (PGG) and poly(2-ethyl-2-oxazoline)-grafted gellan gums (abbreviated as G2, G3, G12) were used as polymeric stabilizing agents of the AuNSs and AuNRs. It was expected that the surface modification of AuNPs with polymers can facilitate their cellular uptake. This enhancement is attributed to the affinity of both natural and synthetic polymers to cellular membranes.[59,60]

UV/Vis-spectroscopy is an effective method for confirming the formation and stabilization of aqueous dispersions of AuNSs and AuNRs. In general, AuNSs possess a single absorption band in the visible (500–550 nm) spectral region, which is known as a surface plasmon resonance (SPR). AuNRs exhibit two major absorption bands corresponding to the transverse and longitudinal SPR bands in the visible (~ 520 nm) and the near-infrared regions, respectively.[57,61] The SPR spectrum is dependent on both the size and shape of gold nanoparticles. In this study, the adsorption spectra of polymer-coated AuNSs and AuNRs dispersions were recorded **(**Figure 1**)**. The spectra confirmed a distinctive SPR band for AuNSs in the visible (~ 530 nm) region (Figure 1A), while two characteristic surface plasmon bands corresponding to the transverse (~ 520 nm, a weaker band in the visible region) and longitudinal (~ 780 nm in NIR region) bands were observed for gold nanorods (Figure 1B).[59,61,62]

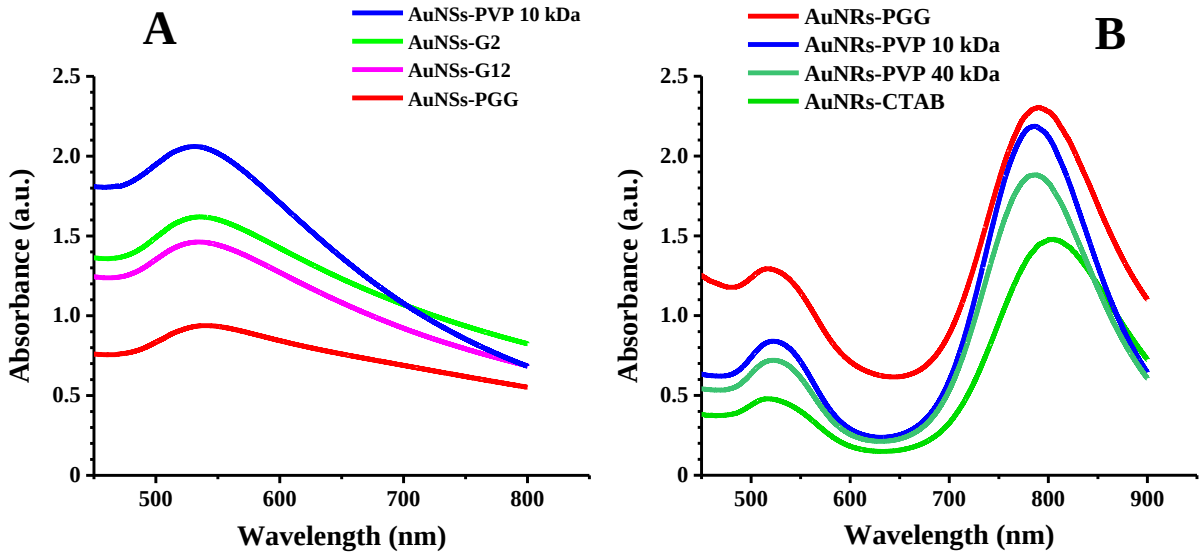

Figure 1. Representative surface plasmon resonance (SPR) absorption bands of spherical (A) and rod-shaped gold nanoparticles (B) stabilized using different amounts of polymers and a surfactant. Pristine gellan gum (PGG, 0.5%); G2 and G12 are poly(2-ethyl-2-oxazoline)-grafted gellan gums with different grafting densities (each at 2%); poly(*N*-vinylpyrrolidone) (PVP) with Mn 10 and 40 kDa (4%), and cetyltrimethylammonium bromide (CTAB, 0.2 M). All spectra were recorded at 25 °C.

Controlling the size of AuNPs is a critical factor in the synthesis of colloidal gold and their application in PTT. Many studies have demonstrated that the interaction between gold nanoparticles and polymers significantly influences the size, stability, and size distributions of the particles.[63,64] Producing monodisperse polymer-coated AuNPs with smaller sizes in aqueous media can lead to improved biocompatibility, reduced cytotoxicity, and enhanced catalytic properties.

The average hydrodynamic size and zeta potential values of the spherical and rod-shaped AuNPs synthesized and stabilized with optimally selected concentrations of synthetic and natural polymers are summarized in Table 1 and Table 2, respectively. During the dialysis, the pH of aqueous solution of AuNPs decreased from 12 to 8 confirming that most of the low-molecular-weight impurities are washed out. The mean diameter and zeta potential values of AuNSs were measured by DLS before and after dialysis against deionized water. It was observed that after dialysis, the size of AuNSs decreased by 2-3 times (Table 1). Overall, most of the spherical gold nanoparticles were polydisperse. The size distributions (before and after dialysis) of spherical gold nanoparticles stabilized with different polymers determined with DLS are shown in Figure S2.

320 Table 1. Size and zeta potential values of polymer-protected AuNSs determined by DLS.

Type of polymer	Concentration of polymer (% w/v)	Mean diameter (nm)				Zeta potential (mV)	
		Before dialysis	PDI	After dialysis	PDI	Before dialysis	After dialysis
PVP 10 kDa	4.0	42 ± 2	0.353	15 ± 1	0.309	–13 ± 2	–19 ± 2
PVP 40 kDa	4.0	47 ± 2	0.225	16 ± 2	0.238	–7 ± 2	–10 ± 3
PGG	0.5	88 ± 2	0.300	37 ± 2	0.415	–32 ± 2	–42 ± 3
G12	2.0	38 ± 1	0.513	13 ± 1	0.795	–21 ± 2	–33 ± 2
G3	2.0	22 ± 1	0.587	17 ± 1	0.671	–20 ± 2	–40 ± 2
G2	2.0	39 ± 1	0.496	11 ± 1	0.496	–18 ± 2	–39 ± 2

321 G2; G3 and G12 – poly(2-ethyl-2-oxazoline)-grafted gellan gums with different grafting densities; PDI –
322 polydispersity index; PGG – pristine gellan gum; PVP – poly(*N*-vinylpyrrolidone). Data are expressed as mean ±
323 standard deviation values (n = 3).

324 In order to estimate the nanoparticles surface charge, the zeta potential values of the
325 different AuNPs were measured. It appears that the zeta potential values of AuNPs significantly
326 decreased following the dialysis, resulting in a further reduction of negative charges. The
327 average zeta potential values of AuNSs were between −42 and −10 mV depending on the
328 polymers used and dialysis (Table 1).
329 AuNRs stabilized using PGG displayed a negative zeta potential (–30 ± 3 mV) value due
330 to the presence of carboxylic groups in the macromolecular chains of the polysaccharide (Table
331 2). Initially, the surface of AuNRs stabilized using PVP 10 and 40 kDa was positively charged,
332 perhaps due to the presence of some excessive counterions of CTAB; however, after dialysis,
333 AuNR's zeta potential decreased down to –7 and –6 mV.

334 Table 2. Aspect ratio (measured using TEM) and zeta potential values of AuNRs synthesized
335 and stabilized using PGG, G2 and PVPs.

Type of polymer	Concentration of polymer (% w/v)	Average length (nm)	Average width (nm)	Aspect ratio	ζ-potential (mV)
CTAB	n/a	42 ± 4	14 ± 2	3 ± 1	54 ± 11
PGG	0.5	34 ± 3	9 ± 2	4 ± 1	–30 ± 3
G2	2.0	53 ± 5	18 ± 3	3 ± 1	– 17 ± 2

PVP 10 kDa	4.0	44 ± 13	15 ± 3	3 ± 1	−7 ± 1
PVP 40 kDa	4.0	55 ± 2	16 ± 1	4 ± 1	–6 ± 2

CTAB – cetyltrimethylammonium bromide; PGG – pristine gellan gum; PVP – poly(*N*-vinylpyrrolidone); n/a – not applicable. Data are presented as mean ± standard deviation (n = 3).

The TEM images (Figure 2) further confirmed the DLS results regarding the size of AuNPs, and both AuNSs and AuNRs were uniformly distributed. For instance, AuNSs in all batches displayed particles with sizes less than 40 nm in diameter. AuNSs stabilized with G2 (GG-*g*-PEtOx) demonstrated even smaller size with 10 ± 1 nm. The aspect ratio, i.e. length/width, for the gold nanorods stabilized using PVP 10 kDa was ~3–4 in average (44 ± 13 nm lengthwise by 15 ± 3 nm in width) and the microphotographs are displayed in Figure 2 (also see Figure S3).

3.1.1. Study of photothermal effects of AuNPs

The photothermal effect (*i.e.* light-to-heat conversion) of AuNSs was studied on porcine stomach tissues as model of skin. The temperature change in tissue samples was measured with an IR thermometer upon irradiation using a 530 nm visible light laser. Visible light was chosen for the current study to avoid unwanted heat stimulation, as it is generally not strongly absorbed by the bulk tissue (Figure 1A). Figure 3 shows the temperature changes in porcine stomach tissue samples with and without injection of polymer-stabilized AuNSs dispersion as a function of irradiation time. The highest temperature recorded was 43.5 ± 0.2 °C for AuNSs–PVP 40 kDa dispersion without tissue sample when exposed to irradiation for 60 min. For the tissue sample containing AuNSs–PVP 40 kDa; PGG and G2 (GG-*g*-PEtOx), the maximum temperature reached up to 41.1 ± 0.2; 41.0 ± 0.2 and 40.7 ± 0.2 °C, respectively, whereas the tissue sample without AuNSs was heated up to 39.0 ± 0.2 °C during 60 min of irradiation. These results clearly indicate that photothermal heating was induced by AuNSs in the tissue samples when exposed to the visible light source.

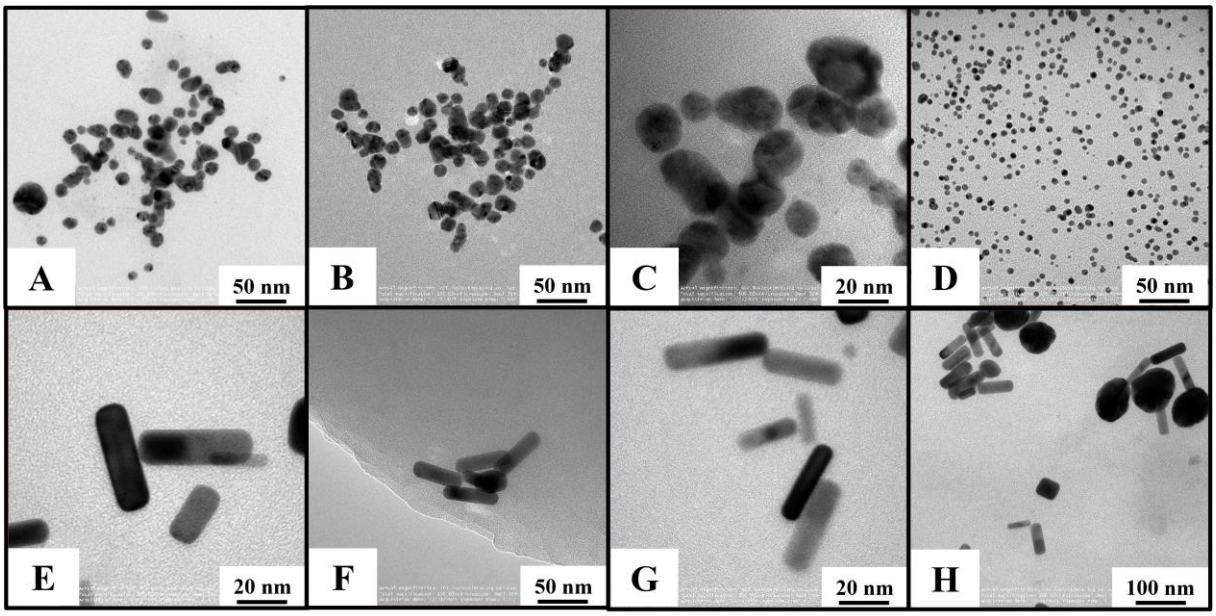

Figure 2. TEM images of AuNSs and AuNRs stabilized using poly(N-vinylpyrrolidone) with Mn 10 kDa (A and E, respectively); poly(N-vinylpyrrolidone) with Mn 40 kDa (B and F, respectively); pristine gellan gum (C and G, respectively); G2 – poly(2-ethyl-2-oxazoline)-grafted gellan gum (D, for spherical gold NPs) and cetyltrimethylammonium bromide without polymer (H, for gold nanorods AuNRs).

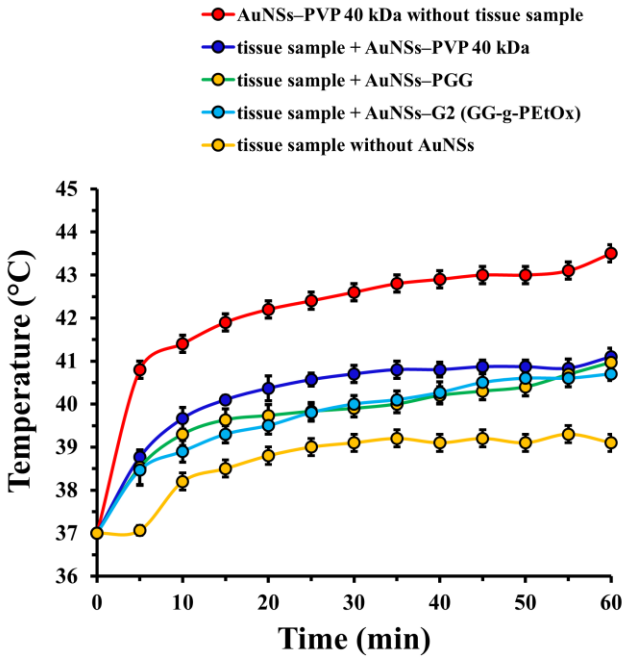

Figure 3. Time-dependent heating curves for AuNSs upon irradiation using a 530 nm visible light source. AuNSs – gold nanospheres; PGG – pristine gellan gum; G2 – poly(2-ethyl-2-oxazoline)-grafted gellan gum; PVP 40 kDa – poly(*N*-vinylpyrrolidone) with Mn 40 kDa.

As seen from Figure 3, aqueous dispersion of AuNSs stabilized by PVP 40 kDa without tissue sample shows higher heating temperature upon irradiation compared to tissue-containing samples at identical conditions. Exact explanation of this phenomenon is complicated because the light-to-heat conversion depends on many parameters, in particular incident laser power, light wavelength, irradiation time, concentration, size and shape of AuNPs.[65] In our mind overall increase in the temperature may be due to a collective heating effect of many nanoparticles within the excitation volume as mentioned by authors.[66] Our results are consistent with data of authors[67] indicating that the cancerous tissues can be overheated above the physiological level (typically 39–45 °C). In our case the heating reaches up to ≈ 40-43°C (ΔT ≈ 3-6 °C). The temperature profiles of colloidal AuNPs solutions (not stabilized by polymers) with different particle sizes were studied.[68] The temperature of the AuNPs solution increased exponentially upon laser illumination (λ = 532 nm), reached the equilibrium after ~ 1200 s, and then returned to the ambient value after discontinuing irradiation. Upon irradiation the system is averagely heated up to 31.5 °C (ΔT ≈ 6.5 °C). Our observations are in good agreement with these results. The photothermal properties of gold nanoparticles, in addition to laser power, light wavelength, irradiation time, concentration, size and shape, depend on various experimental factors, such as stirring, data recording and analysis, and the effective mass of the system. Moreover, in presence of natural tissue, other molecules adsorb 530 nm light (e.g. hemoglobin and myoglobin), which makes the irradiation less effective. However, 530 nm light corresponds to the maximum of SPR and makes research on the photothermal phenomenon more effective. Whereas the 530 nm light is the most appropriate for laboratory tests and basic studies, it is less suitable for work with natural tissues. Short wavelengths are often adsorbed by natural molecules, *e.g*. hemoglobin and myoglobin have absorbance maxima about this value. This decreases effectiveness of the photothermal treatment and one has to work with longer wavelengths. In our case we used 780 nm light, which guaranteed that the studies photothermal effect originates from the light absorbance.

3.1.2. Efficacy of PTT treatment in Ehrlich cancer cells

Ehrlich cancer cells were used to investigate the efficacy of AuNPs-based PTT treatment under the visible light irradiation. Ehrlich tumor is a well-established murine tumor model frequently employed in many cancer researches, both solid and ascitic forms. Classified as a carcinoma, it originates in the epithelial tissue of the skin or lining of internal organs. This tumor was initially derived from a spontaneous mammary adenocarcinoma in a mouse and has since been propagated in various strains of mice. Ehrlich tumor cells exhibit rapid proliferation

and are characterized by their ability to induce ascites fluid accumulation in the peritoneal cavity when injected intraperitoneally. This tumor model is commonly employed to study tumor biology, tumor immunology, anti-cancer drug screening, and evaluating therapeutic interventions. Such attributes as high growth rate, good reproducibility, metastatic potential, and relative stability in morphological and biological characteristics were the reason to use Ehrlich cancer cells in this study.[69–73] In order to assess the potential effect of bio-nano interactions, *in vitro* experiments were performed using an HBSS buffer solution. First, Ehrlich cancer cells were dispersed in a buffer solution at a ratio of 1:9. Then, 1 mL of the suspension of extracted Ehrlich cancer cells was mixed with 1 mL of either polymer-stabilized AuNPs or AuNRs for 5 min. The suspension was irradiated with visible (530 nm) and NIR (780 nm) laser lights for 60 min at an intensity of 10 and 90 mW, respectively. Microphotographs of the cells were then acquired from randomly selected 10 points in a Goryaev chamber and Ehrlich tumor cells in the visible area of the microscope were counted (Figure 4). Interestingly, the number of cells was considerably reduced in the presence of AuNSs stabilized with PVP 40 kDa even without irradiation after 40 days of examination (Figure 4B). An explanation of this phenomenon requires further experiments. No significant cell damage was observed in control experiments without AuNSs, indicating that the membranes were intact and that the cells have not been affected very much during 60 min of laser irradiation. However, due to an increase in the temperature of the medium up to 39 °C when the samples were irradiated with either a visible or NIR light source for 60 min and further inspection during the experimental period, there was some reduction in the number of cells recorded in 40 days. As such there was no statistically significant difference between the numbers recorded in control samples with and without irradiation.

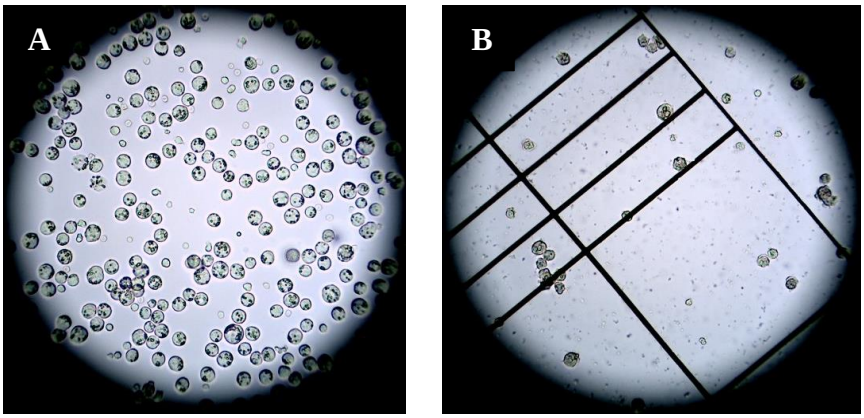

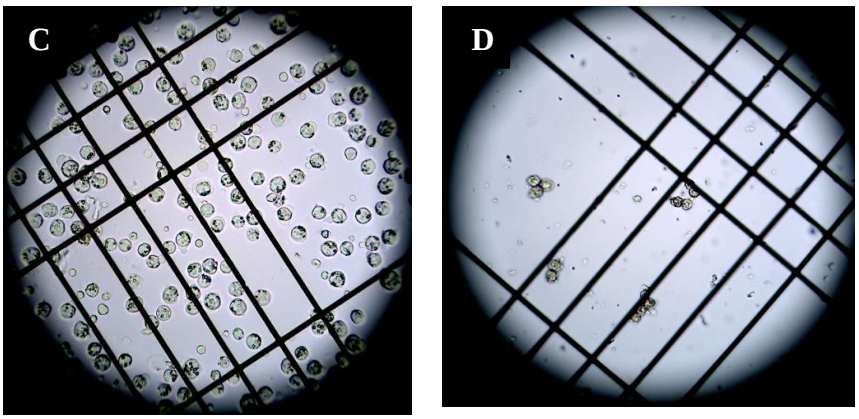

Figure 4. Microphotographs of a suspension of Ehrlich cancer cells irradiated with visible (530 nm) light. (A): before irradiation and without AuNSs; (B): in the presence of AuNSs–PVP 40 kDa with no irradiation (in 40 days). After irradiation and in 40 days: without AuNSs (C), in the presence of AuNSs–PVP 40 kDa (D). PVP 40 kDa – poly(*N*-vinylpyrrolidone) with Mn 40 kDa.

Irradiating cancer cells using visible light at 530 nm in the presence of spherical AuNPs stabilized with polymers and without yielded good results. Figure 5 displays the reduction in the number of cancer cells counted from microphotographs taken from randomly selected 10 points (numerical values are shown in Table S1). For instance, the number of cancer cells counted after 30 – 40 days decreased by 10 – 40 times in comparison with the control samples ($p < 0.0001$). It should be noted that the number of cells in the presence of AuNSs stabilized with polymers was reduced even without irradiation. Probably the gold nanoparticles retard the growth of cancer cells, however, irradiation enhances this process. The true mechanism of this phenomenon is not well understood and will be clarified in subsequent experiments.

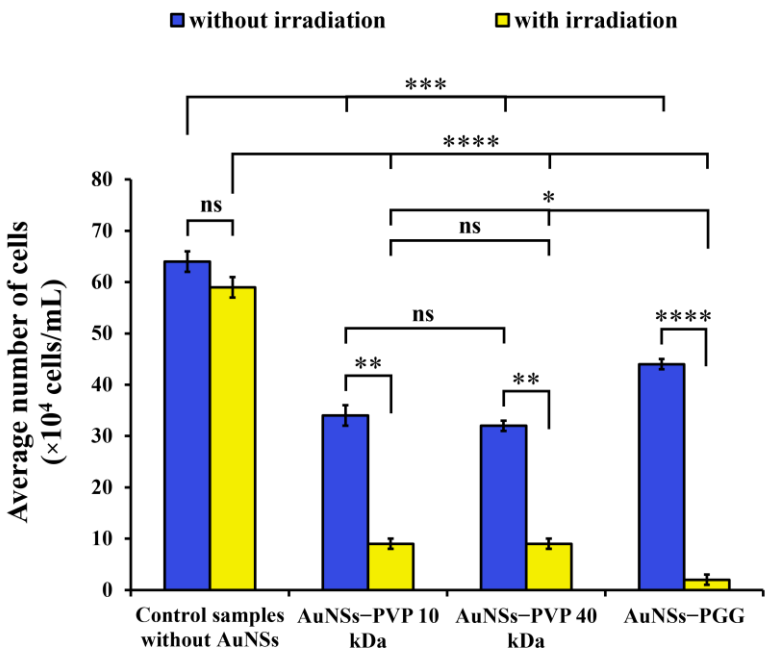

Figure 5. Number of cancer cells in control samples and in the presence of polymers-stabilized AuNSs when exposed to the visible light source at 530 nm and without irradiation. The results are presented after 40 days of examination. Data are expressed as mean ± SEM of triplicate with n = 10 measurements in each. Statistically significant differences are given as: **** = $p < 0.0001$; *** = $p < 0.001$; ** = $p < 0.01$; * = $p < 0.05$; ns denotes no significance. AuNSs – spherical gold nanoparticles; PGG – pristine gellan gum; PVP 10 kDa and 40 kDa – poly(*N*-vinylpyrrolidone) with Mn 10 and 40 kDa, respectively.

Experimental results showing the effects of irradiation on the cancer cells using NIR light at 780 nm in the presence of AuNRs stabilized with polymers and control samples are illustrated in Figure 6 (numerical values are presented in Table S2). The results are presented after 40 days of examination. The number of damaged cancer cells following irradiation increased markedly after 30-40 days of inspection, particularly, there was a statistically significant difference between the numbers recorded for polymer-stabilized AuNRs and control samples without gold nanorods ($p < 0.0001$). At the same time, no statistically significant difference was observed between the samples of AuNRs stabilized with polymers followed by irradiation and in 40 days of observation, demonstrating a similar PTT effect. Numerous studies have shown that gold nanorods with an appropriate dimension (28 × 8 nm) are the most effective for PTT compared to other types of gold nanoparticles, such as nanospheres and nanoshells.[9,56] Despite the AuNRs having slightly larger dimensions in size, as reported in the present work (Table 2),

overall, polymer-coated AuNRs demonstrated good efficacy in PTT treatment *in vitro* and showed a comparable PTT effect as to spherical AuNPs.

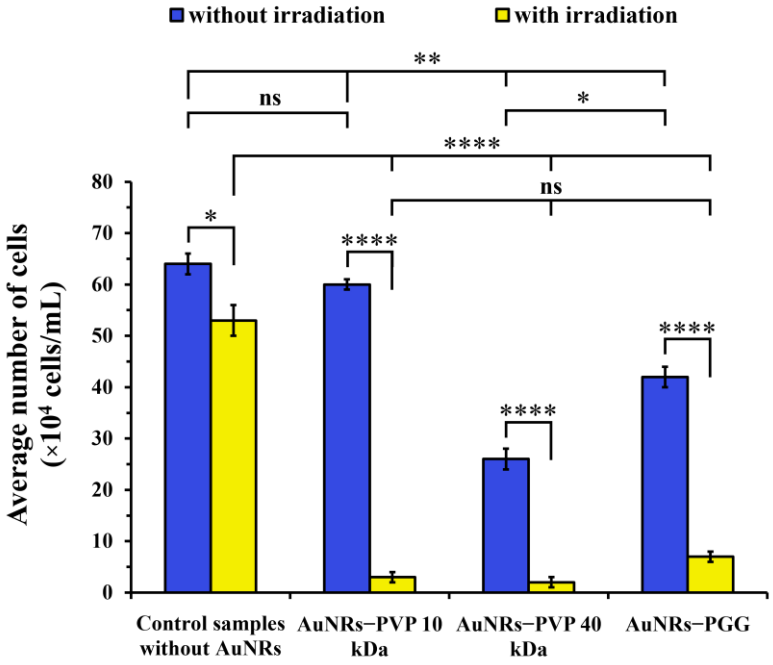

Figure 6. Number of cancer cells in control samples and in the presence of polymer-stabilized AuNRs when exposed to NIR light irradiation at 780 nm and without irradiation. The results are presented after 40 days of examination. Data are expressed as mean ± SEM of triplicate with n = 10 measurements in each. Statistically significant differences are shown as: **** = $p < 0.0001$; ** = $p < 0.01$; * = $p < 0.05$; ns denotes no significance. AuNRs – gold nanorods; PGG – pristine gellan gum; PVP 10 kDa and 40 kDa – poly(*N*-vinylpyrrolidone) with Mn 10 and 40 kDa, respectively.

In our experiments the photothermal conversion efficiency of AuNPs irradiated with 530 and 780 nm laser sources were not evaluated. As seen from Figure 1, for polymer-stabilized AuNSs and AuNRs the adsorption maximums are in the range of 535±5 nm and close to ≈ 800 nm. The physiotherapeutic Lasmik® laser apparatus used for irradiation had only two laser sources with a wavelength of 530 and 780 nm. In case of AuNSs the absorption band at λ ≈ 535±5 nm more or less corresponds to laser light at 530 nm. But the adsorption peaks of AuNRs at λ ≈ 800 nm considerably deviates from the laser light at 780 nm. Probably this is the reason of less efficiency AuNRs in light-to-heat conversion compared to AuNSs. The photothermal conversion efficiency of different shapes of AuNPs under laser irradiation has been reported.[74-77] In particular the photothermal conversion efficiency of gold nanospheres (AuNSs) and gold

nanorods (AuNRs) was evaluated at different irradiation intensities of near-infrared (NIR) broadband (754-816 nm) and NIR laser (808 nm) irradiation.[78] It was shown that the photothermal conversion efficiency of AuNSs and AuNRs is comparable. But the spherical gold nanoparticles might be preferable for hyperthermia applications with a higher accumulation rate within the tumor sites.

3.1.3. In vivo study of the photothermal effect of AuNPs

As the *in vitro* experiments demonstrated successful photothermal destruction of cancer cells in the presence of polymer-stabilized AuNSs under irradiation with visible light, subsequent *in vivo* studies were conducted to evaluate the therapeutic efficacy of this approach further. Tumor development was induced by injecting cancer cells into the left flanks of CD-1 mice subcutaneously (see Figure S4A), after which the tumors were allowed to grow for a period of 10 days. This is consistent with the results of authors [72] because the death of the animal with Ehrlich ascites carcinoma occurs between 10 and 14 days after cell inoculation depending on (I) the concentration of inoculated cells, (II) the amount of fluid in the peritoneal cavity, which causes abdominal pressure and compression of the organs, and (III) the number of passages, in which repeated transplantation increases malignancy and tumor proliferation. Before each exposure, the linear dimensions of the tumors in animals were measured using a caliper (see Figure S4B). The volumes of the tumors were then calculated using the following equation:

$$V = {}^{4}/_{3}\,\pi R^{3} \quad (1)$$

where R is the radius of the tumor, and π is a value equal to 3.14.

Laser irradiation of tumor-bearing mice injected with AuNSs stabilized with PVP 40 kDa demonstrated a remarkable PTT effect (Figure 7). This result shows that further tumor growth is successfully inhibited by AuNSs–PVP injection in combination with a visible light laser irradiation.

Three days following the last exposure (see Figure S4C), the animals were humanely sacrificed, and the tumors were removed and weighed (Figure 8 and Figure S4D). The average tumor weight in the control group was 1.00 ± 0.30 g; in Group 2 with AuNSs–PVP 40 kDa it was 0.54 ± 0.20 g; in Group 3 with AuNSs–PVP 40 kDa and irradiation it was 0.15 ± 0.04 g. Figure 8 shows the comparison between tumor weight in different groups of animals measured when the animals were sacrificed.

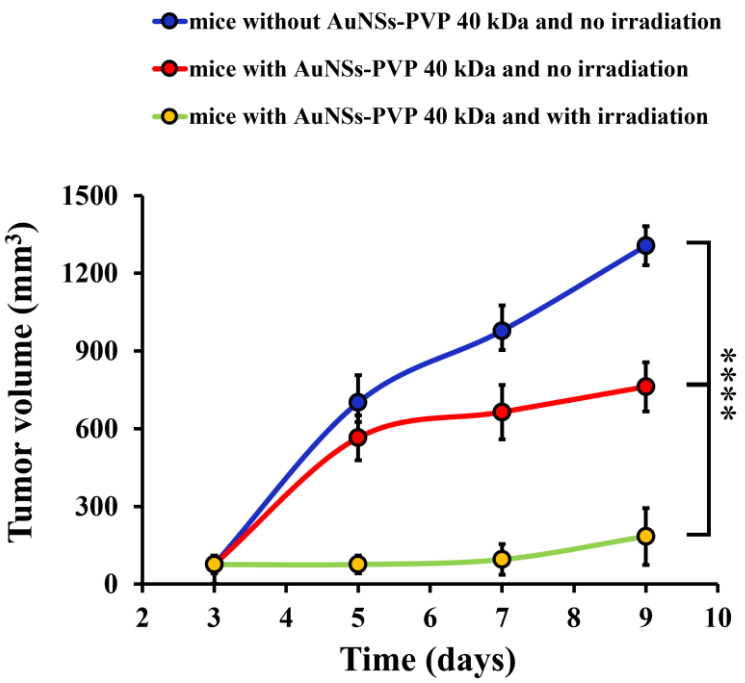

Figure 7. Tumor growth in each treatment group as monitored for 9 days. Data are expressed as mean ± SD values (n = 5). Statistically significant difference is represented as **** = $p < 0.0001$. PVP 40 kDa – poly(*N*-vinylpyrrolidone) with Mn 40 kDa.

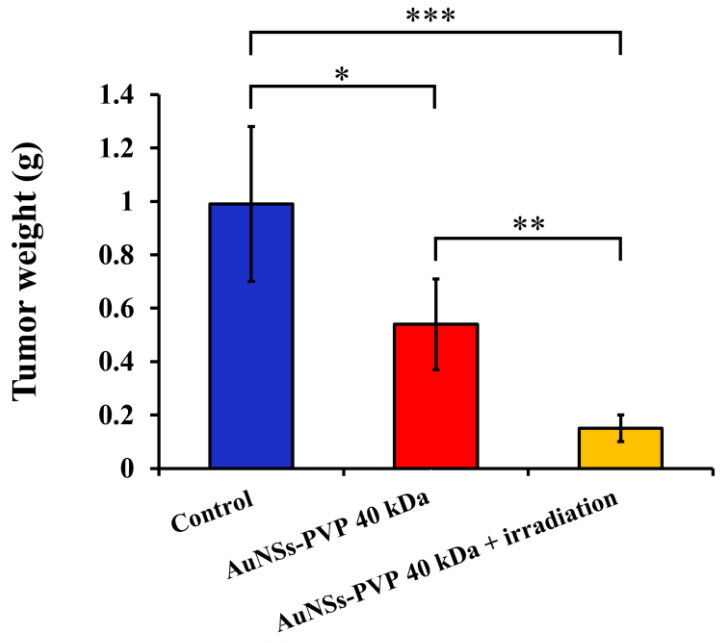

Figure 8. Tumor weight in different groups of animals measured when the animals were sacrificed. Data are produced as mean ± SD (n = 5). Statistically significant differences are represented as: *** = $p < 0.001$; ** = $p < 0.01$; * = $p < 0.05$. PVP 40 kDa – poly(N-vinylpyrrolidone) with Mn 40 kDa.

The tumor growth inhibition coefficient (TGIC) was calculated using the following equation:

$$TGIC = \frac{V_k - V_0}{V_k} \times 100\% \quad (2)$$

where, V_k is the volume (or weight) of the tumor in the control group of animals, and V_0 is the volume (or weight) of the tumor in each experimental group of animals.

The comparison of the sizes of tumors from different groups of mice was performed and the results are summarized in Table 3. The visual inspection of tumor sizes is depicted in Figure S5. Samples with AuNSs–PVP 40 kDa and without irradiation exhibited a reduced tumor growth after 3 days by 19 ± 10%, which was an effect that gradually increased after 7 days, reaching 42 ± 5%. Samples with AuNSs–PVP 40 kDa and with irradiation showed a greater effect with up to 90 ± 6% reduction in the tumor size after 7 days. In 9 days TGIC calculated using the tumor weight in samples with AuNSs–PVP 40 kDa and without irradiation was 43 ± 23% and in samples with AuNSs–PVP 40 kDa plus irradiation reached 85 ± 3%. Based on these results, it can be concluded that the spherical AuNSs stabilized using PVP 40 kDa could be considered as suitable candidates to inhibit Ehrlich tumor growth and could potentially be used in PTT treatment.

Table 3. Inhibition of tumor growth with intratumoral injection of AuNSs–PVP (40 kDa) before and after irradiation at λ = 633 nm.

Samples	Inhibition (%)			
	Tumor volume			Tumor weight
	3 days	5 days	7 days	9 days
AuNSs–PVP 40 kDa without irradiation	19 ± 10	32 ± 12	42 ± 5	43 ± 23
AuNSs–PVP 40 kDa with irradiation	86 ± 8	90 ± 4	90 ± 6	85 ± 3

PVP 40 kDa – poly(*N*-vinylpyrrolidone) with M_n 40 kDa.

4. Conclusion

Spherical and rod-like gold nanoparticles protected with poly(*N*-vinylpyrrolidone), pristine gellan gum, and poly(2-ethyl-2-oxazoline)-grafted gellan gum were prepared and characterized in this study. The gold nanoparticles exhibited the presence of characteristic

surface plasmon resonance (SPR) bands. The nanoparticles were analyzed for their applicability as photothermal therapy (PTT) agents with respect to Ehrlich cancer cells when exposed to the visible light source. Following the dialysis, the average hydrodynamic size of AuNPs reduced by approximately 2-3 times and the zeta potential decreased by ~1.5-2 times, indicating that the AuNPs are suitable for PTT. Experiments with *ex vivo* porcine stomach tissues containing AuNSs were performed to determine the photothermal effect of nanoparticles when exposed to the visible light source. In the course of laser irradiation of the tissue at 530 nm, the highest temperature recorded was 43 ± 0.5 °C for AuNSs stabilized using PVP 40 kDa. *In vitro* experiments demonstrated a similar PTT effect for Ehrlich cancer cells containing polymer-protected AuNPs upon irradiation both at 530 and 780 nm. After 40 days of examination, the number of Ehrlich cancer cells decreased by 10-40 times in comparison with the control samples. *In vivo* experiments on mice revealed that injection of AuNSs–PVP 40 kDa followed by irradiation with visible light considerably decreased the size of tumors, indicating that polymer-stabilized gold nanoparticles could potentially be used in the PTT treatment of Ehrlich tumors. The AuNPs developed and stabilized with polymers in this work might potentially be considered as a platform for the PTT treatment of not only Ehrlich tumors, but also other type of carcinoma. In near perspectives our study may be related to light-to-heat conversion efficiency evaluation of AuNSs and AuNRs, toxicological experiments, study the mucoadhesive properties polymer-protected AuNPs to improve the adhesion to cancer cell, modification the surface of AuNPs with poly(ethyleneglycol) to enhance the cellular uptake, conjugation of AuNPs with the anti-cancer drug doxorubicin *etc*. In future perspectives the "green" synthesis using the natural substances (for instance, bacterium, fungi, and plants) may contribute to reducing and stabilizing agents for the synthesis of AuNPs and enhance their medical properties such as anti-microbial and anti-cancer activity.

Supporting Information

The following supporting information can be downloaded at: www.mdpi.com/xxx/s1. Figure S1: A Lazmik® laser apparatus and the process of tissue irradiation after injection of the polymer-stabilized gold nanoparticles within an incubator; Figure S2: Size distributions (before and after dialysis) of spherical gold nanoparticles stabilized with different polymers determined using DLS; Figure S3: TEM images of polymer-stabilized spherical gold NPs and rod-like gold NPs; Table S1 and Table S2: Number of cancer cells counted in control samples and in the presence of polymer-stabilized AuNSs and AuNRs followed by irradiation with visible light (530 nm) and NIR light (780 nm) sources, respectively, and results are presented during 40 days

of examination; Figure S4: The process of injection of colloidal AuNSs into mice, measuring the tumor size, irradiating the tumor with a light source, and tumor removal from an animal; Figure S5: Visual comparison of the sizes of tumor samples removed from different groups of mice.

Acknowledgements

This research was funded by the Science Committee of the Ministry of Education and Science of the Republic of Kazakhstan (Grant No. AP13067773) and was supported by the Horizon 2020 research and innovation program of the European Union Maria Sklodowska-Curie (grant agreement 823883-NanoPol-MSCA-RISE-2018).

Received: ((will be filled in by the editorial staff))
Revised: ((will be filled in by the editorial staff))
Published online: ((will be filled in by the editorial staff))

References

1. Peng, J.; Liang, X.; Calderon, L. Progress in research on gold nanoparticles in cancer management. *Medicine (Baltimore).* **2019**, *98*, e15311.
2. Yang, Z.; Sun, Z.; Ren, Y.; Chen, X.; Zhang, W.; Zhu, X.; Mao, Z.; Shen, J.; Nie, S. Advances in nanomaterials for use in photothermal and photodynamic therapeutics (Review). *Mol. Med. Rep.* **2019**, *20*, 5–15.
3. *World Cancer Report: Cancer Research for Cancer Prevention*; Wild, C.P., Weiderpass, E., Stewart, B.W., Eds.; International Agency for Research on Cancer: Lyon, France, 2020; ISBN 978-92-832-0447-3.
4. Han, H.S.; Choi, K.Y. Advances in nanomaterial-mediated photothermal cancer therapies: Toward clinical applications. *Biomedicines* **2021**, *9*, 305.
5. Vines, J.B.; Yoon, J.-H.; Ryu, N.-E.; Lim, D.-J.; Park, H. Gold nanoparticles for photothermal cancer therapy. *Front. Chem.* **2019**, *7*, 167.
6. Costantini, P.E.; Di Giosia, M.; Ulfo, L.; Petrosino, A.; Saporetti, R.; Fimognari, C.; Pompa, P.P.; Danielli, A.; Turrini, E.; Boselli, L.; et al. Spiky gold nanoparticles for the photothermal eradication of colon cancer cells. *Nanomaterials* **2021**, *11*, 1608.
7. Zhao, N.; Pan, Y.; Cheng, Z.; Liu, H. Gold nanoparticles for cancer theranostics — A brief update. *J. Innov. Opt. Health Sci.* **2016**, *9*, 1630004.
8. Lee, J.; Lee, Y.H.; Jeong, C.B.; Choi, J.S.; Chang, K.S.; Yoon, M. Gold nanorods-conjugated TiO2 nanoclusters for the synergistic combination of phototherapeutic treatments of cancer cells. *J. Nanobiotechnology* **2018**, *16*, 104.
9. Mackey, M.A.; Ali, M.R.K.; Austin, L.A.; Near, R.D.; El-Sayed, M.A. The most effective gold nanorod size for plasmonic photothermal therapy: Theory and in vitro experiments. *J. Phys. Chem. B* **2014**, *118*, 1319–1326.
10. Fratoddi, I.; Venditti, I.; Cametti, C.; Russo, M. V Gold nanoparticles and gold nanoparticle-conjugates for delivery of therapeutic molecules. Progress and challenges. *J. Mater. Chem. B* **2014**, *2*, 4204–4220.
11. Jaque, D.; Martínez Maestro, L.; del Rosal, B.; Haro-Gonzalez, P.; Benayas, A.; Plaza, J.L.; Martín Rodríguez, E.; García Solé, J. Nanoparticles for photothermal therapies. *Nanoscale* **2014**, *6*, 9494–9530.
12. Mendes, R.; Pedrosa, P.; Lima, J.C.; Fernandes, A.R.; Baptista, P. V Photothermal enhancement of chemotherapy in breast cancer by visible irradiation of gold nanoparticles. *Sci. Rep.* **2017**, *7*, 10872.
13. Wang, S.; Lu, G. Applications of Gold Nanoparticles in Cancer Imaging and Treatment. In *Noble and Precious Metals - Properties, Nanoscale Effects and Applications*; Seehra, M.S., Bristow, A.D., Eds.; IntechOpen: London, 2017; pp. 291–309 ISBN 978-1-78923-293-6.
14. Kim, H.S.; Lee, D.Y. Near-infrared-responsive cancer photothermal and photodynamic therapy using gold nanoparticles. *Polymers (Basel).* **2018**, *10*, 961.
15. Yeh, Y.-C.; Creran, B.; Rotello, V.M. Gold nanoparticles: preparation, properties, and applications in bionanotechnology. *Nanoscale* **2012**, *4*, 1871–1880.
16. Ali, M.R.K.; Ibrahim, I.M.; Ali, H.R.; Selim, S.A.; El-Sayed, M.A. Treatment of natural mammary gland tumors in canines and felines using gold nanorods-assisted plasmonic photothermal therapy to induce tumor apoptosis. *Int. J. Nanomedicine* **2016**, *11*, 4849–4863.
17. Riley, R.S.; Day, E.S. Gold nanoparticle-mediated photothermal therapy: applications and opportunities for multimodal cancer treatment. *WIREs Nanomedicine and Nanobiotechnology* **2017**, *9*, e1449.
18. Cai, W.; Gao, T.; Hong, H.; Sun, J. Applications of gold nanoparticles in cancer nanotechnology. *Nanotechnol. Sci. Appl.* **2008**, *1*, 17–32.
19. Ayala-Orozco, C.; Urban, C.; Knight, M.W.; Urban, A.S.; Neumann, O.; Bishnoi, S.W.;

Mukherjee, S.; Goodman, A.M.; Charron, H.; Mitchell, T.; et al. Au Nanomatryoshkas as Efficient Near-Infrared Photothermal Transducers for Cancer Treatment: Benchmarking against Nanoshells. *ACS Nano* **2014**, *8*, 6372–6381.

20. Yao, C.; Zhang, L.; Wang, J.; He, Y.; Xin, J.; Wang, S.; Xu, H.; Zhang, Z. Gold nanoparticle mediated phototherapy for cancer. *J. Nanomater.* **2016**, *2016*, 5497136.
21. Peer, D.; Karp, J.M.; Hong, S.; Farokhzad, O.C.; Margalit, R.; Langer, R. Nanocarriers as an emerging platform for cancer therapy. *Nat. Nanotechnol.* **2007**, *2*, 751–760.
22. Jabeen, F.; Najam-ul-Haq, M.; Javeed, R.; Huck, C.W.; Bonn, G.K. Au-nanomaterials as a superior choice for near-infrared photothermal therapy. *Molecules.* **2014**, *19*, 20580–20593.
23. Wang, J.; Bai, R.; Yang, R.; Liu, J.; Tang, J.; Liu, Y.; Li, J.; Chai, Z.; Chen, C. Size- and surface chemistry-dependent pharmacokinetics and tumor accumulation of engineered gold nanoparticles after intravenous administration. *Metallomics* **2015**, *7*, 516–524.
24. Singh, P.; Pandit, S.; Mokkapati, V.R.S.S.; Garg, A.; Ravikumar, V.; Mijakovic, I. Gold nanoparticles in diagnostics and therapeutics for human c ancer. *Int. J. Mol. Sci.* **2018**, *19*, 1979.
25. Huang, X.; El-Sayed, M.A. Gold nanoparticles: Optical properties and implementations in cancer diagnosis and photothermal therapy. *J. Adv. Res.* **2010**, *1*, 13–28.
26. Jain, S.; Hirst, D.G.; O'Sullivan, J.M. Gold nanoparticles as novel agents for cancer therapy. *Br. J. Radiol.* **2012**, *85*, 101–113.
27. Cabral, R.M.; Baptista, P. V The chemistry and biology of gold nanoparticle-mediated photothermal therapy: Promises and challenges. *Nano Life* **2013**, *3*, 1330001.
28. Guerrero-Florez, V.; Mendez-Sanchez, S.C.; Patrón-Soberano, O.A.; Rodríguez-González, V.; Blach, D.; Martínez O., F. Gold nanoparticle-mediated generation of reactive oxygen species during plasmonic photothermal therapy: a comparative study for different particle sizes, shapes, and surface conjugations. *J. Mater. Chem. B* **2020**, *8*, 2862–2875.
29. Conde, J. et al. Gold-nanobeacons for gene therapy: evaluation of genotoxicity, cell toxicity and proteome profiling analysis. *Nanotoxicology* **2014**, 8, 521–532.
30. Conde, J.; Rosa, J.; Baptista, P. Gold-Nanobeacons as a theranostic system for the detection and inhibition of specific genes. *Protoc. Exch.* **2013**, 1–35.
31. Jain, S.; Hirst, D.G.; O'Sullivan, J. M. Gold nanoparticles as novel agents for cancer therapy. *Br. J. Radiol.* **2012,** 85, 101–13.
32. Qin, Z.; Wang, Y.; Randrianalisoa, J.; Raeesi, V. et al. Quantitative Comparison of Photothermal Heat Generation between Gold Nanospheres and Nanorods. *Sci. Rep*. **2016**, 6, 1–13.
33. Cabral, R. M.; Baptista, P. V. Anti-cancer precision theranostics: a focus on multifunctional gold nanoparticles. *Expert Rev. Mol. Diagn.* **2014**,14, 1–12.
34. Huang, X.; El-Sayed, M. A. Gold nanoparticles: Optical properties and implementations in cancer diagnosis and photothermal therapy. *J. Adv. Res.* **2010**,1, 13–28.
35 Dumur, F.; Guerlin, A.; Dumas, E.; Bertin, D.; Gigmes, D.; Mayer, C.R. Controlled spontaneous generation of gold nanoparticles assisted by dual reducing and capping agents. *Gold Bull.* **2011**, *44*, 119–137.
36. Yah, C.S. The toxicity of Gold Nanoparticles in relation to their physiochemical properties. *Biomed. Res.* **2013**, *24*, 400–413.
37. Zhang, Y.; Zhan, X.; Xiong, J.; Peng, S.; Huang, W.; Joshi, R.; Cai, Y.; Liu, Y.; Li, R.; Yuan, K.; et al. Temperature-dependent cell death patterns induced by functionalized gold nanoparticle photothermal therapy in melanoma cells. *Sci. Rep.* **2018**, *8*, 8720.
38. Liu, Y.; Ai, K.; Liu, J.; Deng, M.; He, Y.; Lu, L. Dopamine-Melanin Colloidal Nanospheres: An Efficient Near-Infrared Photothermal Therapeutic Agent for *in vivo* Cancer Therapy. *Adv. Mater.* **2013**, *25*, 1353–1359.

39. Li, W.; Rong, P.; Yang, K.; Huang, P.; Sun, K.; Chen, X. Semimetal nanomaterials of antimony as highly efficient agent for photoacoustic imaging and photothermal therapy. *Biomaterials.* **2015**, *45*, 18–26.
40. Amatya, R.; Hwang, S.; Park, T.; Min, K.A.; Shin, M.C. *In vitro* and *in vivo* Evaluation of PEGylated Starch-Coated Iron Oxide Nanoparticles for Enhanced Photothermal Cancer Therapy. *Pharmaceutics.* **2021**, *13*, 871.
41. Bucharskaya, A.B.; Maslyakova, G.N.; Afanasyeva, G.A.; Terentyuk, G.S.; Navolokin, N.A.; Zlobina, O. V; Chumakov, D.S.; Bashkatov, A.N.; Genina, E.A.; Khlebtsov, N.G.; et al. The morpho-functional assessment of plasmonic photothermal therapy effects on transplanted liver tumor. *J. Innov. Opt. Health Sci.* **2015**, *8*, 1541004.
42. Dhar, S.; Maheswara Reddy, E.; Shiras, A.; Pokharkar, V.; Prasad, B.L.V. Natural gum reduced/stabilized gold nanoparticles for drug delivery formulations. *Chem. - A Eur. J.* **2008**, *14*, 10244–10250.
43. Dhar, S.; Mali, V.; Bodhankar, S.; Shiras, A.; Prasad, B.L.V.; Pokharkar, V. Biocompatible gellan gum-reduced gold nanoparticles: Cellular uptake and subacute oral toxicity studies. *J. Appl. Toxicol.* **2011**, *31*, 411–420.
44. Dhar, S.; Reddy, E.M.; Prabhune, A.; Pokharkar, V.; Shiras, A.; Prasad, B.L.V. Cytotoxicity of sophorolipid-gellan gum-gold nanoparticle conjugates and their doxorubicin loaded derivatives towards human glioma and human glioma stem cell lines. *Nanoscale.* **2011**, *3*, 575–580.
45. D'Arrigo, G.; Di Meo, C.; Gaucci, E.; Chichiarelli, S.; Coviello, T.; Capitani, D.; Alhaique, F.; Matricardi, P. Self-assembled gellan-based nanohydrogels as a tool for prednisolone delivery. *Soft Matter.* **2012**, *8*, 11557–11564.
46. D'Arrigo, G.; Navarro, G.; Di Meo, C.; Matricardi, P.; Torchilin, V. Gellan gum nanohydrogel containing anti-inflammatory and anti-cancer drugs: A multi-drug delivery system for a combination therapy in cancer treatment. *Eur. J. Pharm. Biopharm.* **2014**, *87*, 208–216.
47. Reis, C.A.; Rodrigues, C.F.; Moreira, A.F.; Jacinto, T.A.; Ferreira, P.; Correia, I.J. Development of gold-core silica shell nanospheres coated with poly-2-ethyl-oxazoline and β-cyclodextrin aimed for cancer therapy. *Mater. Sci. Eng. C* **2019**, *98*, 960–968.
48. Kudaibergenov, S.E.; Xu, S.; Tatykhanova, G.S.; Kudaibergenova, G.M. Gellan Gum Immobilized Anticancer Drugs and Gold Nanoparticles in Nanomedicine. *Acad. J. Polym. Sci.* **2019**, *2*, 555588.
49. Soleimani, K.; Derakhshankhah, H.; Jaymand, M.; Samadian, H. Stimuli-responsive natural gums-based drug delivery systems for cancer treatment. *Carbohydr. Polym.* **2021**, *254*, 117422.
50. Nurgaziyeva, E.; Kudaibergenov, S.; Mun, G.; Khutoryanskiy, V. Synthesis of fluorescently-labelled poly(2-ethyl-2-oxazoline)-protected gold nanoparticles. *Chem. Bull. Kazakh Natl. Univ.* **2021**, *100*, 12–20.
51. Agsish, N.D.; Fedoroff S. Tumor cell population of the Ehrlich ascites tumors. *Can. J. Genet. Cytol.* **1968**, 10, 723-746.
52. Badr El-Din, N.K.; Shabana, S.M.; Abdulmajeed, B.A.; Ghoneum, M. A novel kefir product (PFT) inhibits Ehrlich ascites carcinoma in mice via induction of apoptosis and immunomodulation. *BMC Complementary Medicine and Therapies.* **2020,** 20, 127.
53. Niemelä, E.; Desai, D.; Nkizinkiko, Y.; Eriksson, J.E.; Rosenholm, J.M. Sugar-decorated mesoporous silica nanoparticles as delivery vehicles for the poorly soluble drug celastrol enables targeted induction of apoptosis in cancer cells. *Eur. J. Pharm. Biopharm.* **2015**, *96*, 11–21.
54. Agibayeva, L.E.; Kaldybekov, D.B.; Porfiryeva, N.N.; Garipova, V.R.; Mangazbayeva, R.A.; Moustafine, R.I.; Semina, I.I.; Mun, G.A.; Kudaibergenov, S.E.; Khutoryanskiy, V. V. Gellan gum and its methacrylated derivatives as in situ gelling mucoadhesive

formulations of pilocarpine: In vitro and in vivo studies. *Int. J. Pharm.* **2020**, *577*, 119093.
55. Ways, T.M.M.; Filippov, S.K.; Maji, S.; Glassner, M.; Cegłowski, M.; Hoogenboom, R.; King, S.; Lau, W.M.; Khutoryanskiy, V. V. Mucus-penetrating nanoparticles based on chitosan grafted with various non-ionic polymers: Synthesis, structural characterisation and diffusion studies. *J. Colloid Interface Sci.* **2022**, *626*, 251–264.
56. Lavikainen, J.; Dauletbekova, M.; Toleutay, G.; Kaliva, M.; Chatzinikolaidou, M.; Kudaibergenov, S. E.; Tenkovtsev, A.; Khutoryanskiy, V. V.; Vamvakaki, M.; Aseyev, V. Poly(2-ethyl-2-oxazoline) grafted gellan gum for potential application in transmucosal drug delivery. *Polym. Adv. Technol.* **2021**, 32, 2770-2780.
57. Nurakhmetova, Z. A.; Azhkeyeva, A. N.; Klassen, I. A.; Tatykhanova, G.S. Synthesis and Stabilization of Gold Nanoparticles Using Water-Soluble Synthetic and Natural Polymers. *Polymers (Basel)* **2020**, 12, 2625.
58. Aljohani, H.; Khodier, A. E.; Al-Gayyar, M. M. Antitumor Activity of Luteolin Against Ehrlich Solid Carcinoma in Rats via Blocking Wnt/β-Catenin/SMAD4 Pathway. *Cureus.* **2023**, 15, e39789.
59. Shan, J.; Tenhu, H. Recent advances in polymer protected gold nanoparticles: synthesis, properties and applications. *Chem. Commun.* **2007**, 44, 4580-4598.
60. Li, X.; Guo, J.; Asong, J.; Wolfert, M.A.; Boons, G.J. Development of Bioorthogonal Reactions and Their Applications in Bioconjugation. *J. Am. Chem. Soc.* **2011**, 133, 11147-11153.
61. Bingham, J. M.; Willets, K. A.; Shah, N. C.; Andrews, D. Q.; Van Duyne, R. P. Localized surface plasmon resonance imaging: Simultaneous single nanoparticle spectroscopy and diffusional dynamics. *J. Phys. Chem. C* **2009**, 113, 16839-16842.
62. Chen, H.; Kou, X.; Yang, Z.; Ni, W.; Wang, J. Shape- and Size-Dependent Refractive Index Sensitivity of Gold Nanoparticles. *Langmuir* **2008**, 24, 5233-5237.
63. Shenhar, R.; Norsten, T.B.; Rotello, V.M. Polymer-mediated nanoparticle assembly: Structural control and applications. *Adv. Mater.* **2005**, 17, 657-669.
64. Sengani, M.; Grumezescu, A. M.; Rajeswari, V. D. Recent trends and methodologies in gold nanoparticle synthesis – A prospective review on drug delivery aspect. *OpenNano*. **2017**, 2, 37-46.
65. Roper, D.K.; Ahn, W.; Hoepfner, M. Microscale Heat transfer transduced by surface plasmon resonant gold nanoparticles. *J. Phys. Chem.* C. **2007**,111(9), 3636–3641.
66. Richardson, H.H.; Carlson, M.T.; Tandler, P.J.; Hernandez, P.; Govorov, A.O. Experimental and theoretical studies of light-to-heat conversion and collective heating effects in metal nanoparticle solutions. *Nano Lett*. **2009**, 9(3), 1139-46.
67. Van der Zee, J.; Vujaskovic, Z.; Kondo, M.; Sugahara, T. The Kadota Fund International Forum 2004-Clinical Group Consensus. *Int. J. Hyperthermia*. **2008**, 24 (2), 111−122
68. Jiang, K.; Smith, D. A.; Pinchuk, A. Size-dependent photothermal conversion efficiencies of plasmonically heated gold nanoparticles. J. Phys. Chem. C 2013, 117 (51), 27073 – 27080
69. Patt, H.M.; Straube, R.L.; Ann, N.Y. Measurement and nature of ascites tumor growth *Acad. Sci.* **1956**, 63, 728-737.
70. Ryzhova, N. I.; Deryagina, V. P.; Savluchinskaya, L. A. The value of the model of ehrlich adenocarcinoma in the study of the mechanisms of carcinogenesis, and antitumor activity of chemical and physical factors. *Int. J. Appl. Fundam. Res.* **2019**, 4, 220-227.
71. Abd Eldaim, M. A.; Tousson, E.; El Sayed, I. E. T.; Abd Elmaksoud, A. Z.; Ahmed, A. A. S. Ameliorative effects of 9-diaminoacridine derivative against Ehrlich ascites carcinoma-induced hepatorenal injury in mice. *Environ. Sci. Pollut. Res.* **2021**, 28, 21835-21850.
72. Radulski, D.R.; Stipp, M.C.; Galindo, C.M.; Acco, A. Features and applications of Ehrlich tumor model in cancer studies: a literature review. *Transl. Breast Cancer Res.*

2023, *4*, 22.
73. Lim, W. Q.; Gao, Z. Plasmonic nanoparticles in biomedicine. *Nano Today.* **2016**, 11, 168-188.
74. Diallo, A. T.; Tlemçani, M.; Khan, M.; Spadavecchia, J.; Djaker, N. size, shape, and wavelength effect on photothermal heat elevation of gold nanoparticles: Absorption coefficient experimental measurement. *Part. Part. Syst. Charact.* **2020**, 37, 2000255.
75. Ma, K.; Li, Y.; Wang, Z.; Chen, Y.; Zhang, X.; Chen, C.; Yu, H.;Huang, J.; Yang, Z.; Wang, X.; Wang, Z. Core−shell gold nanorod@layered double hydroxide nanomaterial with highly efficient photothermal conversion and its application in antibacterial and tumor therapy. *ACS Appl. Mater. Interfaces.* **2019**, 11, 29630–29640.
76. Zhou, J.; Jiang, Y.; Hou, S.; Upputuri, P. K.; Wu, D.; Li, J.; Wang, P.; Zhen, X.; Pramanik, M.; Pu, K.; Duan, H. Compact plasmonic blackbody for cancer theranosis in the Near-Infrared II window. *ACS-Nano*. **2018**, 12, 2643–2651.
77. Alrahili, M.; Peroor, R.; Savchuk, V.; McNear, K.; Pinchuk, A. Morphology dependence in photothermal heating of gold nanomaterials with Near-Infrared Laser. *J. Phys. Chem. C.* **2020**, 124, 4755–4763.
78. Vikas; Kumar, R.; Sanjeev, S. Concentration-dependent photothermal conversion efficiency of gold nanoparticles under Near-Infrared Laser and broadband irradiation. *Beilstein J. Nanotechnol.* **2023**, 14, 205–217.

815 **TOC**
816

The spherical (AuNSs) and rod-like gold nanoparticles (AuNRs) are stabilized by poly(N-vinylpyrrolidone), pristine gellan gum, and poly(2-ethyl-2-oxazoline)-grafted gellan gum. Polymer-protected AuNSs and AuNRs suppress the growth of Ehrlich cancer cells by 10-40 times compared to the control. *In vivo* experiments demonstrate a significant decrease in tumor size of mice after injection of AuNSs–PVP 40 kDa and irradiation with visible light.

G.S. Tatykhanova[1,3,*], R.N. Tuleyeva[1,2], Zh.A. Nurakhmetova[1], N.N. Gizatullina[1], V.K. Krasnoshtanov[4], D.B. Kaldybekov[1,2,6], V.O. Aseyev[5], V.V. Khutoryanskiy[6], S.E. Kudaibergenov[1*].

Polymer-protected gold nanoparticles for photothermal treatment of Ehrlich adenocarcinoma: in vitro and in vivo studies

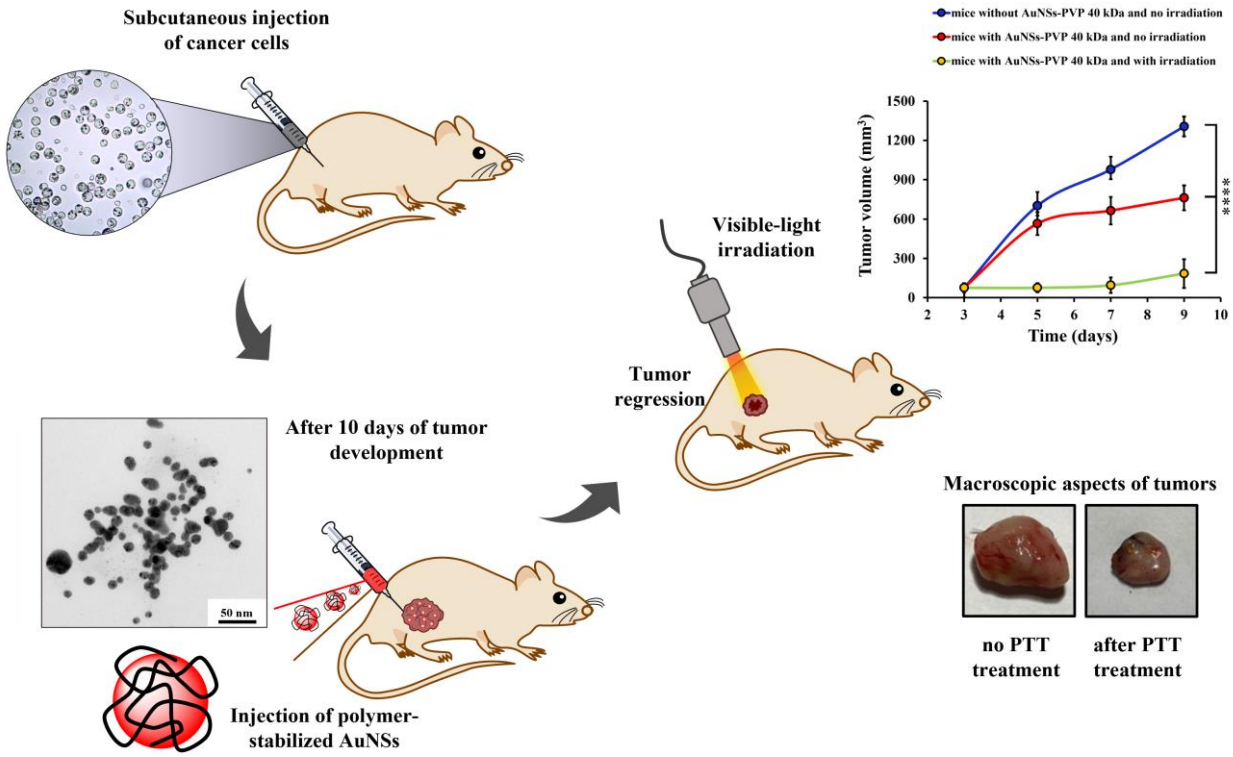

Supporting Information

Polymer-protected gold nanoparticles for photothermal treatment of Ehrlich adenocarcinoma: in vitro and in vivo studies

Gulnur S. Tatykhanova[1,3], Rysgul N. Tuleyeva[1,2], Zhanara A. Nurakhmetova[1], Nargiz N. Gizatullina[1], Vladimir K. Krasnoshtanov[4], Daulet B. Kaldybekov[1,2,6] , Vladimir O. Aseyev[5], Vitaliy V. Khutoryanskiy[6], Sarkyt E. Kudaibergenov[1*]*

[1] Institute of Polymer Materials and Technology, 050019 Almaty, Kazakhstan

[2] Department of Chemistry and Chemical Technology, Al-Farabi Kazakh National University, 050040 Almaty, Kazakhstan

[3] Satbayev University, 050013 Almaty, Kazakhstan

[4] Kazakh Research Institute of Oncology and Radiology, 050022 Almaty, Kazakhstan

[5] Department of Chemistry, University of Helsinki, 00014 Helsinki, Finland

[6] Reading School of Pharmacy, University of Reading, Whiteknights, RG6 6DX Reading, United Kingdom

Irradiation of polymer-coated gold nanoparticles was carried out using a physiotherapeutic laser apparatus Lazmik® (Moscow, Russia) (Figure S1A). Experiments were carried out within an incubator that maintained appropriate temperature and humidity (Figure S1B).

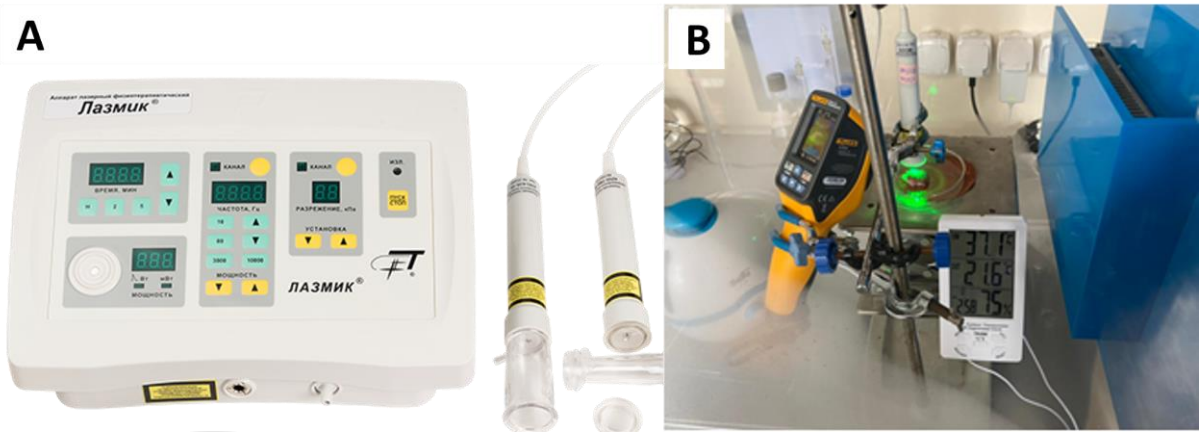

Figure S1. A Lazmik® laser apparatus (A) and the process of tissue irradiation after injection of the polymer-stabilized gold nanoparticles within an incubator (B).

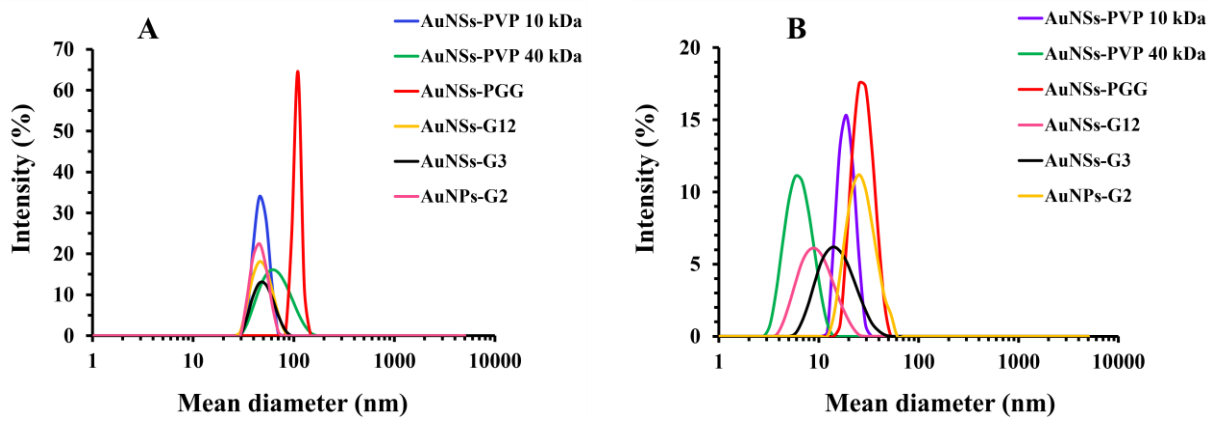

Figure S2. Size distributions of spherical gold nanoparticles stabilized with different polymers as determined by DLS; before (A) and after dialysis (B).

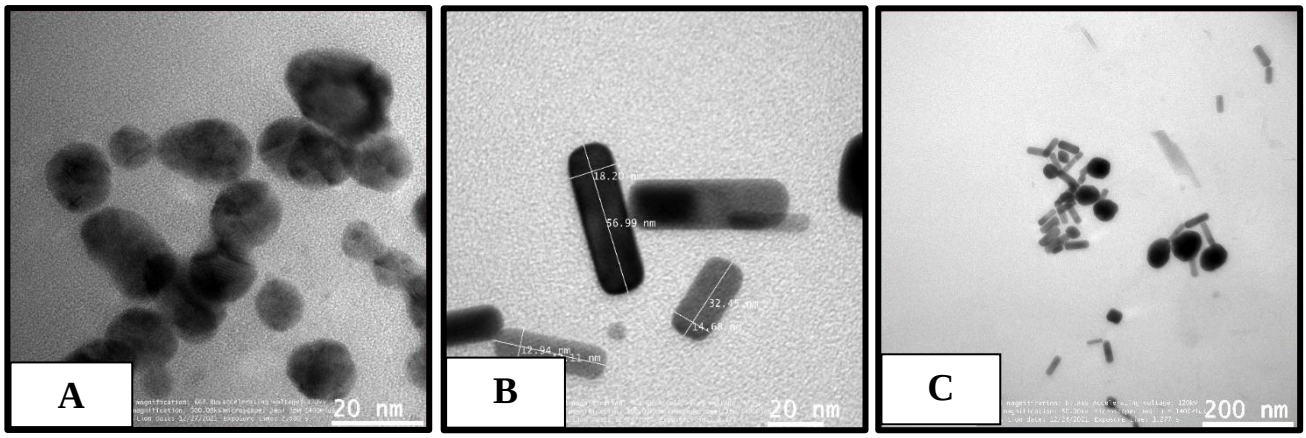

Figure S3. TEM images of spherical gold NPs stabilized using pristine gellan gum (A); rod-like gold NPs stabilized using PVP 10 kDa (B) and G2 – poly(2-ethyl-2-oxazoline)-grafted gellan gum (C).

Table S1. Number of cancer cells counted in control samples and in the presence of AuNSs stabilized using PVP 10 and 40 kDa and PGG followed by irradiation with a visible light source at 530 nm and results are presented during 40 days of examination.

Days	Control samples without AuNSs		AuNSs–PVP 10 kDa		AuNSs–PVP 40 kDa		AuNSs–PGG	
	without irradiation	with irradiation	without irradiation	with irradiation	without irradiation	with irradiation	without irradiation	with irradiation
0	202 ± 1	202 ± 1	120 ± 1	98 ± 1	79 ± 1	96 ± 2	77 ± 1	112 ± 1
1	190 ± 2	196 ± 1	92 ± 1	96 ± 1	71 ± 1	92 ± 1	77 ± 1	77 ± 1
5	158 ± 2	173 ± 1	71 ± 1	6 ± 1	65 ± 1	29 ± 1	65 ± 1	7 ± 1
10	131 ± 1	164 ± 1	62 ± 1	9 ± 1	62 ± 1	20 ± 2	60 ± 1	5 ± 1
15	130 ± 1	153 ± 1	55 ± 2	8 ± 1	50 ± 1	19 ± 1	56 ± 1	9 ± 1
20	76 ± 1	131 ± 1	47 ± 1	14 ± 2	46 ± 1	19 ± 1	48 ± 1	7 ± 1
30	94 ± 1	140 ± 1	36 ± 1	19 ± 1	33 ± 1	7 ± 1	46 ± 1	5 ± 1
40	64 ± 2	59 ± 2	34 ± 2	9 ± 1	32 ± 1	9 ± 1	44 ± 1	2 ± 1

Data are expressed as mean ± SEM (n = 10) of triplicate.

Table S2. Number of cancer cells counted in control samples and in the presence of AuNRs stabilized using PVP 10 and 40 kDa and PGG followed by irradiation with a near-infrared (NIR) light source at 780 nm and results are presented during 40 days of examination.

Days	Control samples without AuNRs		AuNRs–PVP 10 kDa		AuNRs–PVP 40 kDa		AuNRs–PGG	
	without irradiation	with irradiation	without irradiation	with irradiation	without irradiation	with irradiation	without irradiation	with irradiation
0	202 ± 1	202 ± 1	107 ± 3	118 ± 4	97 ± 4	107 ± 3	92 ± 4	87 ± 5
1	190 ± 2	191 ± 1	89 ± 6	93 ± 4	90 ± 6	95 ± 2	80 ± 3	53 ± 1
5	158 ± 2	161 ± 1	79 ± 3	59 ± 3	71 ± 3	53 ± 2	75 ± 2	49 ± 1
10	131 ± 1	157 ± 1	73 ± 3	50 ± 1	68 ± 2	28 ± 2	60 ± 2	32 ± 1
15	130 ± 1	123 ± 1	73 ± 2	29± 1	68 ± 3	20 ± 2	56 ± 1	24 ± 2
20	76 ± 1	101 ± 1	68 ± 2	15 ± 1	44 ± 4	8 ± 1	56 ± 1	11 ± 1
30	94 ± 1	43 ± 3	62 ± 2	4 ± 1	42 ± 3	3 ± 1	54 ± 1	8 ± 1
40	64 ± 2	53 ± 3	60 ± 1	3 ± 1	26 ± 2	2 ± 1	42 ± 2	7 ± 1

Data are expressed as mean ± SEM (n = 10) of triplicate.

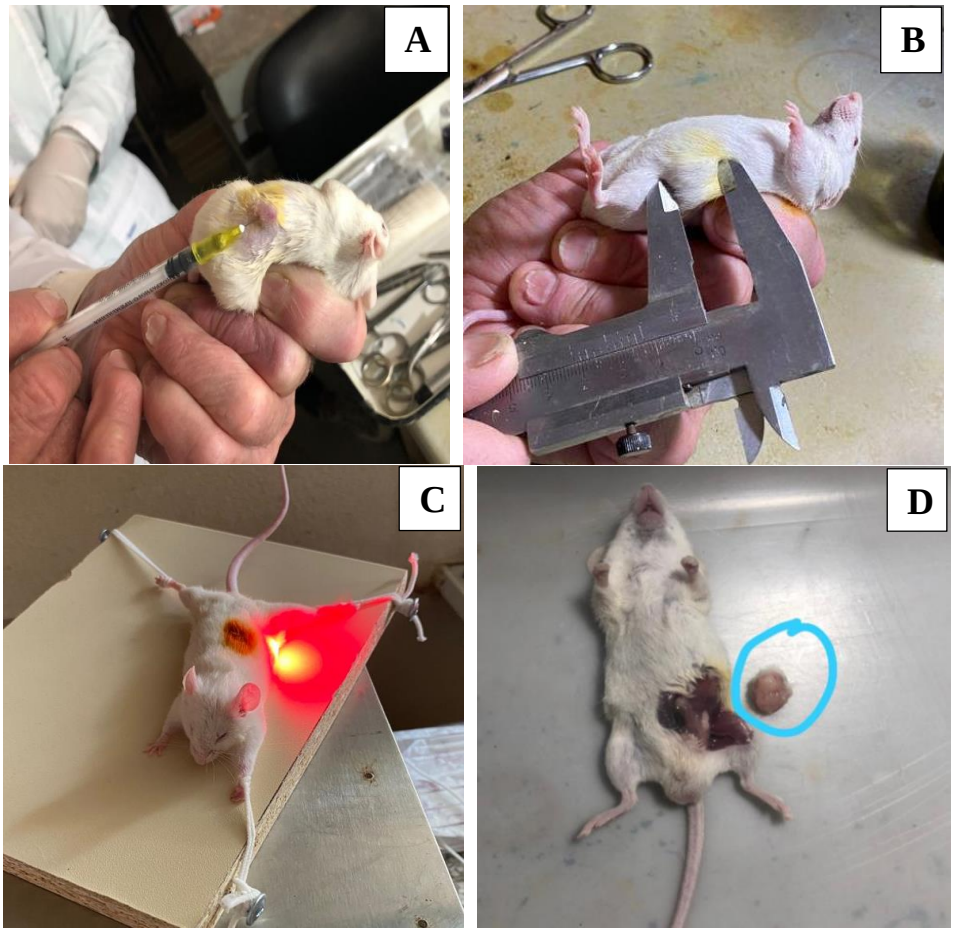

Figure S4. Injection of AuNSs–PVP 40 kDa into the left flanks of mice (A); measuring the tumor size using a caliper (B); irradiating the tumor using a laser light source at λ = 633 nm (C); tumor removal by dissecting the peritoneum (D).

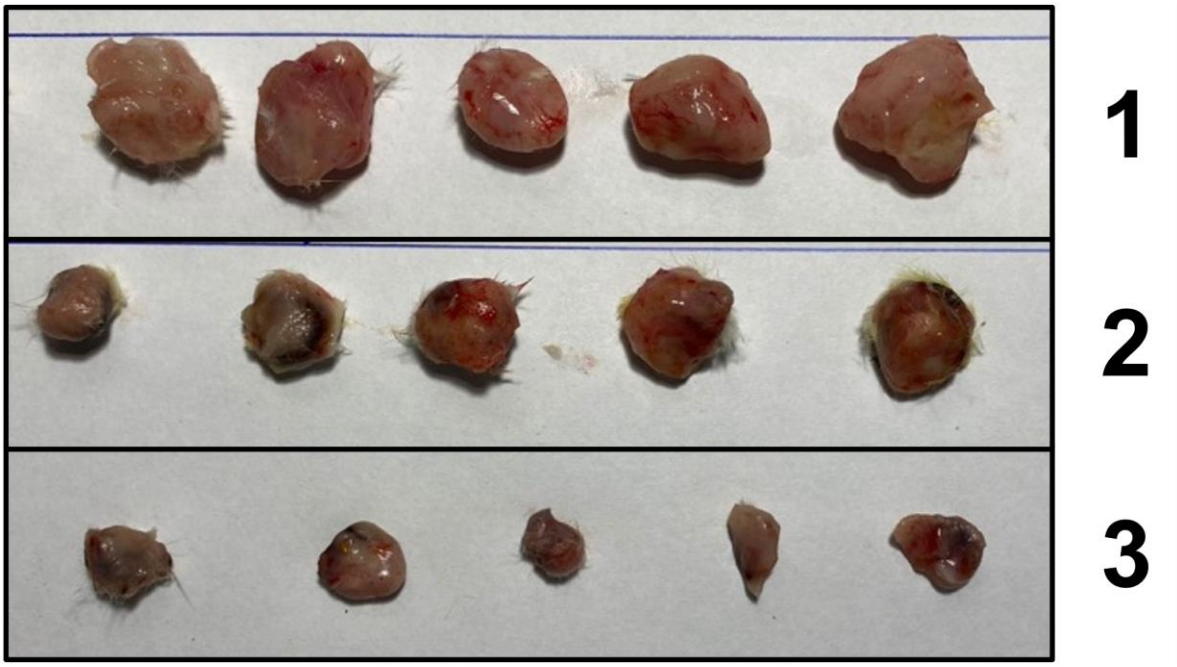

Figure S5. Visual comparison of the sizes of tumor samples removed from different groups of mice. Row 1: Tumor samples taken from the Control group, without injection of AuNSs–PVP 40 kDa and no irradiation; Row 2: Tumor samples taken after injection of AuNSs–PVP 40 kDa and no irradiation; Row 3: Tumor samples taken after injection of AuNSs–PVP 40 kDa and irradiation with $\lambda = 633$ nm light source.